Spec. Publs. int. Ass. Sediment. (2001) **31**, 121–134

Two-dimensional and axisymmetric models for compositional and particle-driven gravity currents in uniform ambient flows

A. J. HOGG* *and* H. E. HUPPERT†

* *Centre for Environmental and Geophysical Flows, School of Mathematics, University of Bristol, University Walk, Bristol BS8 1TW; and*
† *Institute of Theoretical Geophysics, Department of Applied Mathematics and Theoretical Physics, University of Cambridge, Silver Street, Cambridge CB3 9EW, UK*

ABSTRACT

The propagation and dispersion of compositional and particle-driven gravity currents intruding into a uniform ambient flow are analysed. Both two-dimensional (line source) and axisymmetric (point source) releases are investigated. Appropriate theoretical models to describe both the fluid motion and resulting deposit density distribution are developed. We show that the behaviour of the current depends on a non-dimensional parameter that represents the ratio of the advected flux of the ambient flow to the downward particle flux to the boundary. Relationships for the maximum upstream penetration distance are derived in terms of that parameter. The theoretical results are compared successfully with data from laboratory experiments for the upstream and downstream lengths of the current as functions of time, the final density of deposit on the floor and the maximum upstream penetration of the current. A few numerical examples are discussed.

INTRODUCTION

Particle-laden flows play an important role in many different natural and industrial situations. Due to the density difference between the particles and surrounding fluid, the particulate matter is not only advected with the flow but also sediments through it. This relative motion both influences the evolution of the flow and also determines the deposition pattern of the particulate matter.

Most studies of particulate flows have concentrated on situations in which the ambient fluid is quiescent, and much has recently been uncovered about the flow of particle-laden gravity currents intruding into a less dense, otherwise quiescent ambient (see, for example, Simpson, 1997 or Huppert, 1998 for reviews of these situations). The aim of the present contribution is to consider the advection by and sedimentation from a particle-laden current intruding into an ambient which is moving with a uniform horizontal speed far from the current. Such a flow could result in a channel from an applied horizontal pressure gradient, or could represent tidal motions in the ocean, or winds in the atmosphere. The results will thus be relevant to pollution discharge in channels (Huppert, 1997), turbidite formation in the oceans (Dade & Huppert, 1994) and the dispersion of either ash from a volcanic cloud (Ernst *et al.*, 2001) or metalliferous particles from hydrothermal plumes (Baker *et al.*, 1995).

The chapter considers two different geometrical situations: two-dimensional and axisymmetric. Put another way, we consider the influence of a uniform ambient flow on a line release and a point source release of particulate matter. The resulting flow could be followed (in all probability) by solving the relevant shallow-water equations. Instead we develop simpler, but powerful 'box-models' in which horizontal variations within the current at any particular time are ignored (Huppert & Simpson, 1980; Dade & Huppert, 1994). There is generally good agreement between the results of such box models and the more rigorous shallow-water approach (Hallworth *et al.*, 1998). In addition, the link between such integral models and the shallow-water equations has been recently uncovered by Hogg *et al.*

(2000). In the box-model formulation, the presence of an ambient flow can be eliminated by considering a frame of reference that translates uniformly downstream with velocity U. Within that frame the current spreads as if in a quiescent medium, in either a two-dimensional or axisymmetrical fashion as appropriate. However, especially in the axisymmetric situation, the radial spreading in a uniformly translating frame can lead to rather complicated patterns when viewed in the fixed frame (of the stationary floor).

Here we first consider the evolution of compositional currents where the density difference is due to a dissolved component, such as salt. This sets up part of the theoretical framework needed to analyse particle-driven currents, which are then described in detail. Experimental verification of the quantitative theoretical results is then presented, followed by a similar treatment of theoretical aspects of the axisymmetric situation. The main conclusion of our study, along with a brief summary and some practical applications, appear in the discussion and conclusions.

TWO-DIMENSIONAL BOX MODEL

The dynamics of large-scale intrusions of dense fluid, spreading over an impermeable, rigid horizontal boundary, are modelled by balancing inertial and buoyancy forces. Such a theoretical approach has been employed by a number of investigations of buoyancy-driven phenomena in both laboratory and natural environments (Simpson, 1997). It is necessary to include the influence of viscous forces only when the current has spread over a considerable distance and becomes sufficiently thin that an appropriate Reynolds number is less than 2.25 (Bonnecaze *et al.*, 1993). The motion of buoyancy-driven intrusions is predominantly horizontal since the vertical accelerations are negligible. This observation has been exploited in the development of mathematical models of the flow which successfully reproduce the experimental measurements (e.g. Rottman & Simpson, 1983; Bonnecaze *et al.*, 1993). However it is possible to derive a simpler representation of the flow which avoids the need for numerical solution of partial-differential equations and yet produces results in good agreement with the experiments. The intrusion is analysed on the assumption that at all times the salt concentration, or particle distribution, and the height of the current are uniform in the horizontal direction (e.g. Dade & Huppert, 1994; Hallworth *et al.*, 1998). The resulting description is termed a box-model representation because the shape of the current is represented by an evolving series of rectangular boxes. In the following subsections, following Hallworth *et al.* (1998), we derive the box models appropriate to compositional and particle-driven flows in the presence of a uniform mean flow, which inhibits propagation upstream and promotes propagation downstream.

Compositional currents

We consider the instantaneous intrusion of a finite volume V of fluid with a density ρ_c into an ambient fluid of lower density ρ_a. The intruding fluid spreads in a two-dimensional manner along the horizontal boundary underlying the ambient fluid, its motion being driven by gravity acting on the density difference. The ambient fluid flows uniformly in a horizontal direction. The gravity currents spread in both the downstream (x) and the upstream (y) directions, as indicated in Fig. 1(a).

On the assumption that there is no entrainment of ambient fluid into the gravity current, the conservation of volume may be written as

$$l \equiv x + y = A/h, \tag{1}$$

where l is the total length of the current, A is the volume per unit width and h is the thickness of the current, which is assumed to be uniform along the current in this box-model formulation. Conditions on each of x and y (or more accurately, their rates of change) link the frontal velocity with both the ambient velocity and the local wave velocity based on the excess density of the current. (These are the Froude number condition which was studied theoretically by Benjamin (1968) and experimentally by Huppert and Simpson (1980).) Hence we may write that

$$\frac{\mathrm{d}x}{\mathrm{d}t} = U + \mathrm{Fr}(g'h)^{\frac{1}{2}} \qquad \text{and} \qquad \frac{\mathrm{d}y}{\mathrm{d}t} = -U + \mathrm{Fr}(g'h)^{\frac{1}{2}}, \tag{2a, b}$$

where $g' \equiv (\rho_c - \rho_a)g/\rho_a$ is the reduced gravity of the current, U is the mean velocity experienced by the current in the x direction and Fr is the Froude number which is assumed constant and equal to 1.19 (Huppert & Simpson, 1980). Previous studies have suggested that the velocity U is a factor of 0.6 times that of the vertically-averaged ambient flow (Simpson & Britter, 1980 and see the experimental section below).

Integrating Eqs (1) and (2), subject to the initial conditions that $x = y = 0$, we obtain

$$x = Ut + \gamma t^{\frac{2}{3}} \qquad \text{and} \qquad y = -Ut + \gamma t^{\frac{2}{3}}, \tag{3a, b}$$

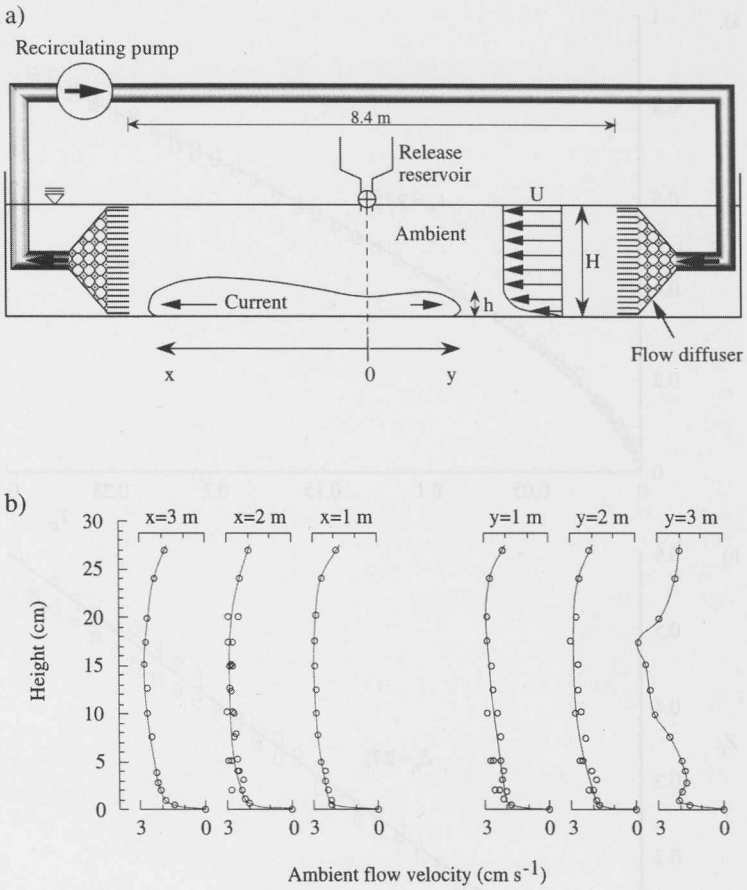

Fig. 1. (a) Schematic diagram of the experimental apparatus (not to scale). (b) Profiles of the horizontal downstream ambient fluid velocity as a function of depth, measured by acoustic Doppler velocimetry at various distances either side of the release position along the medial plane of the flow channel (in the absence of gravity currents). The structure in the profile at $y = 3$ m is due to the proximity of this section to the input diffuser box.

where

$$\gamma = \tfrac{1}{2}(3\mathrm{Fr})^{\frac{2}{3}}(g'A)^{\frac{1}{3}}. \tag{4}$$

By differentiating Eq. (3b) we predict that the maximum distance upstream that the current propagates is given by $\frac{1}{6}\mathrm{Fr}^2(g'A/U^2)$, which except for the pre-multiplicative constant can be quite simply obtained by dimensional analysis.

Inspection of Eq. (3a, b) indicates that there is a timescale

$$\tau_c = (\gamma/U)^3, \tag{5}$$

which corresponds to when the buoyancy-related and ambient velocities are comparable. For times less than τ_c the current propagates mainly due to buoyancy, and the effects of the external flow make a smaller contribution; for times in excess of τ_c external flow effects are more important than the buoyancy. In the experiments described below, this timescale is approximately 200 s, whereas a typical duration of an experimental run was around 60 s, beyond which the gravity current became too thin and weak to be distinguished against the background flow. (After this time the Reynolds number of the current was also too small for the above theory to be appropriate: using the results in appendix B of Bonnecaze *et al.* (1993), obtained by balancing forces, we can evaluate the appropriate Reynolds number as $(A^2/\gamma^2\nu)t^{-\frac{7}{3}}$, where ν is the coefficient of kinematic viscosity. Bonnecaze *et al.* (1993) show that viscous forces dominate the flow when this Reynolds number falls below a value of approximately 2). It was thus impossible for us to test robustly both of the terms of Eq. (3) (in the form written).

It is therefore worthwhile concentrating on the alternative representation

$$l \equiv x + y = 2\gamma t^{\frac{2}{3}} \qquad \text{and} \qquad z \equiv x - y = 2Ut, \tag{6a, b}$$

which evaluate the evolution of the length and twice

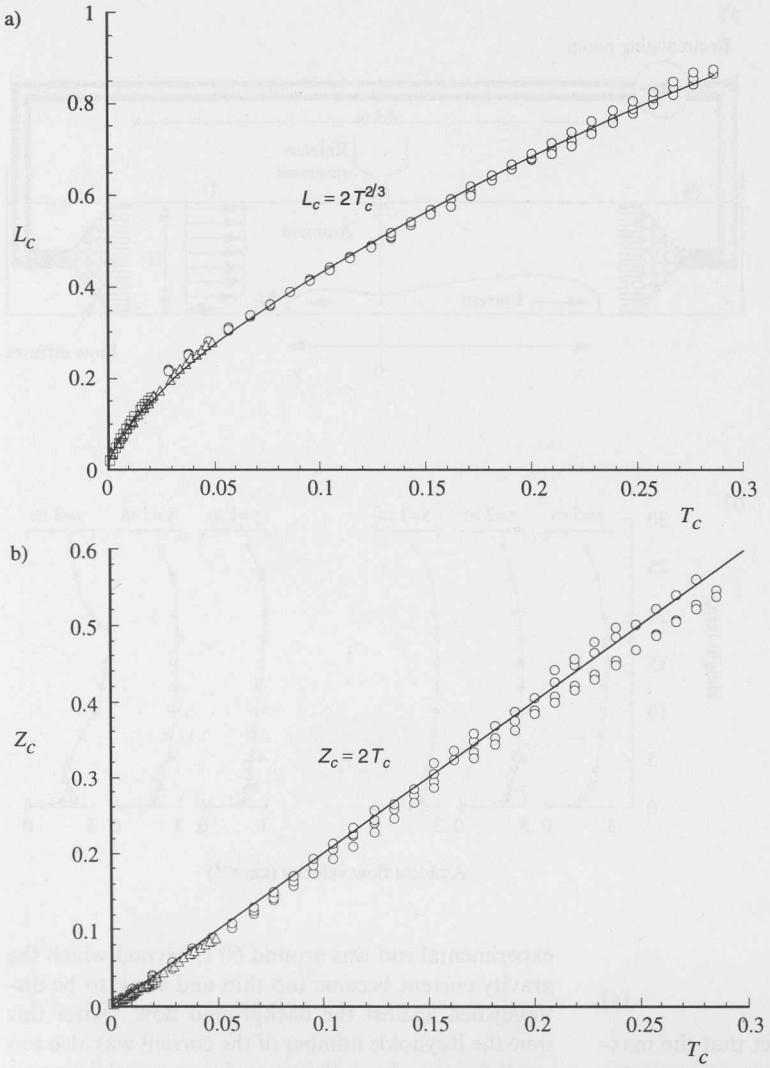

Fig. 2. (a) Non-dimensional length L_c, and (b) non-dimensional position of the centroid Z_c, plotted against nondimensional time T_c, for compositional currents of 50 g, (○), 200 g (△) and 400 g (□) of salt dissolved in 2 litres of water, released into an ambient flow. The theoretical predictions are shown as solid lines in each graph.

the displacement of the centroid from its initial position. Introducing the lengthscale

$$l_c = \gamma^3/U^2 \tag{7}$$

and the non-dimensional variables

$$L_c = l/l_c \qquad Z_c = (x-y)/l_c \qquad \text{and} \qquad T_c = t/\tau_c, \tag{8a, b, c}$$

we plot all our experimental data in Fig. 2 and compare these to our theoretical predictions

$$L_c = 2T_c^{\frac{2}{3}} \qquad \text{and} \qquad Z_c = 2T_c. \tag{9a, b}$$

We note that the non-dimensionalization of the experimental data which allows it to be collapsed so successfully requires the velocity U to be 0.6 $\bar{U}$, the value of the mean ambient flow. The statement that a gravity current only experiences 0.6 of the mean flow has been suggested previously by Simpson and Britter (1980) and in this study we find further strong experimental evidence of this relationship (see below). We note that Eq. (9) indicates that the total length of the current increases as the two-thirds power of the time while the centre of the current propagates downstream at 0.6 times that of the ambient velocity.

Particle-driven currents

The development of a box model for the propagation

of a monodisperse particle current is similar to that for a compositional current. However its density is progressively reduced due to particle sedimentation, which in turn leads to a reduction in flow speed. The Froude number conditions are now written as

$$\frac{\mathrm{d}x}{\mathrm{d}t} = U + \mathrm{Fr}(g'_p \phi h)^{\frac{1}{2}} \quad \text{and} \quad \frac{\mathrm{d}y}{\mathrm{d}t} = -U + \mathrm{Fr}(g'_p \phi h)^{\frac{1}{2}}, \tag{10a, b}$$

where ϕ is the volume fraction of particles and $g'_p \equiv (\rho_s - \rho_a)g/\rho_a$ is the reduced gravity of the particulate phase which has density ρ_s. The sedimentation of particles from the vertically well-mixed current though a basal viscous boundary layer is modelled by a constant settling velocity, V_s, on the assumption that the deposited particles are not re-entrained

$$\frac{\mathrm{d}(\phi A)}{\mathrm{d}t} = -V_s \phi l. \tag{11}$$

The system of Eqs (10) and (11), together with an expression for the conservation of mass (Eq. 1), are integrated subject to the initial conditions $x = y = 0$ and $\phi = \phi_0$. Identifying the dimensionless length and timescales

$$l_\infty = \left[\frac{10\mathrm{Fr}(g'_p \phi_0 A^3)^{\frac{1}{2}}}{V_s}\right]^{\frac{2}{5}} \quad \text{and} \quad \tau_\infty = \frac{5A}{l_\infty V_s} \tag{12a, b}$$

which are then used to define L, $\bar{Z}$ and T as the non-dimensional variables for the length, twice the displacement of the centroid and time, we obtain the relationships (in terms of the variable of integration s)

$$\frac{\phi}{\phi_0} = (1 - L^{\frac{5}{2}})^2, \tag{13a}$$

$$T = \int_0^L \frac{s^{\frac{1}{2}}\,\mathrm{d}s}{1 - s^{\frac{5}{2}}} \equiv \mathcal{F}(L) \tag{13b}$$

and

$$\bar{Z} = \Lambda T, \tag{13c}$$

which are graphed in Fig. 3 along with our experimental data.

In these expressions there remains a single non-dimensional parameter

$$\Lambda = \frac{10UA}{l_\infty^2 V_s}. \tag{14}$$

In contrast to the compositional situation (see above), the current ceases ($\phi = 0$) when $l = l_\infty$, a value that is independent of the ambient flow speed, though we see from Eq. (13b) that this length takes (theoretically) an infinite time to achieve. The magnitude of Λ represents the influence of the mean flow on the runout of the gravity current and is proportional to the ratio of the mean flow to the settling velocity of the particles. More precisely, if we re-write A as the product of the runout length l_∞ and the height of the fluid layer when this length is attained, $A = h_\infty l_\infty$, then the parameter Λ may be seen to represent the ratio of the horizontal flux of fluid, Uh_∞, to the vertical settling flux of particles, $V_s l_\infty$. When the settling flux is large compared to the flux of the mean flow (and thus Λ is much less than unity), the evolution of the gravity current is only weakly affected by the motion of the ambient. Conversely, when Λ is much greater than unity, the gravity current is strongly influenced by the mean flow.

The distribution of the deposit arising from these particle-driven gravity currents may be calculated from the box model analysis on the assumption that the particles sediment out of the current uniformly along its length. When there is no ambient flow, the gravity current propagates symmetrically in the upstream and downstream directions until it attains the maximum length (l_∞). In contrast, when there is an ambient flow, the centroid of the current is advected downstream (cf. Eq. (13c)). Thus the resulting deposit is asymmetric about the initiation line of the two-dimensional current and extends over a considerable distance downstream. The deposit, expressed as the integrated mass flux per unit area delivered to the bottom while the current is overhead, is given by

$$\eta(x) = \rho_p V_s \int_{t_s}^{t_f} \phi\,\mathrm{d}t, \tag{15}$$

where the limits of this integral correspond to the times at which deposition starts and finishes, denoted by t_s and t_f, respectively. We reiterate that a box model of the gravity current is being used in which there is uniform sedimentation along its entire length. Furthermore the length of the box is increasing whilst its centroid is advected downstream. Therefore at a particular location deposition starts when a front of the current first passes and ceases when the rear of the current is swept by. Substituting Eq. (12a, b) into Eq. (15), we obtain the implicit relationship

$$\eta(x) = \frac{5\phi_0 \rho_p A}{l_\infty}\left[\frac{2L^{\frac{3}{2}}}{3} - \frac{L^4}{4}\right]_{L_s}^{L_f}, \tag{16}$$

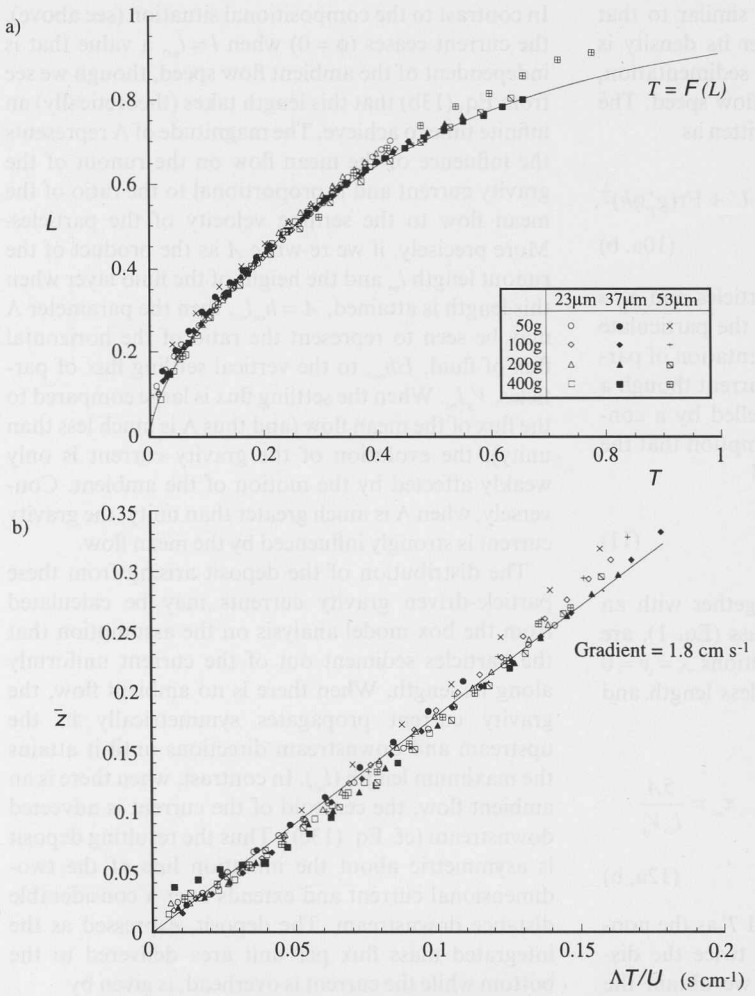

Fig. 3. (a) Non-dimensional length L plotted against nondimensional time T, and (b) non-dimensional position of centroid $\bar{z}$, plotted against $\Lambda T/U$, for particle currents with various masses and sizes of particles (given by legend) initially suspended in 2 litres of water, released into an ambient flow. The solid curve in (a) is the theoretical relationship given by Eq. (13b). The solid curve in (b) is the best-fit straight line through all the data, the gradient of which determines U.

where L_s and L_f are the values of the dimensionless length L at non-dimensional times of T_s and T_f, which correspond to the dimensional times t_s and t_f.

We plot some illustrative profiles of the deposit as a function of position for a range of values of Λ in Figs 4 and 5. As notes above, when there is no ambient flow, $U = \Lambda = 0$, the deposit distribution is symmetric about the point at which the suspension of particles is released. However, as the magnitude of the ambient flow increases relative to the settling velocity of the particles, the profiles become increasingly asymmetric.

Using this simple model of the deposit, we can straightforwardly calculate numerically the maximum upstream distance, d_+, over which the current propagates, as a function of Λ. We present the results in Fig. 6 and find very good agreement between the theoretical curve and the experimental observations (except at $\Lambda = 0$, corresponding to zero flow, the situation in which the maximum upstream point is not as sharply defined, as is seen from Fig. 4). From Eqs (12c) and (16) it is possible to calculate asymptotic representations of this maximum upstream distance in the regimes $\Lambda << 1$ and $\Lambda >> 1$. Using these expansions we may formulate an approximate composite expansion which is given by

$$\frac{d_+}{l_\infty} = \frac{\frac{1}{2} + (\frac{1}{5}\log\Lambda - \frac{\pi}{8})\Lambda + \frac{1}{50}\Lambda^2}{1 + \frac{3}{25}\Lambda^4}, \qquad (17)$$

which is indistinguishable from the full numerical solution.

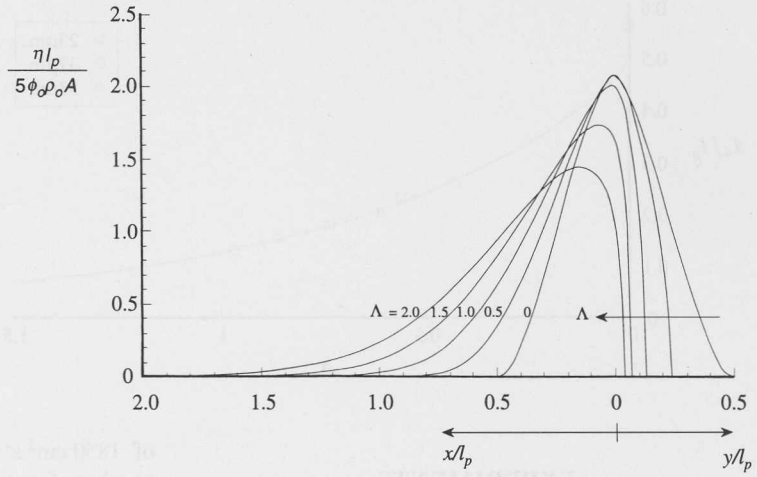

Fig. 4. Non-dimensional deposit thickness as a function of position for a range of values of $\Lambda = 10UA/(V_s l_p^2)$.

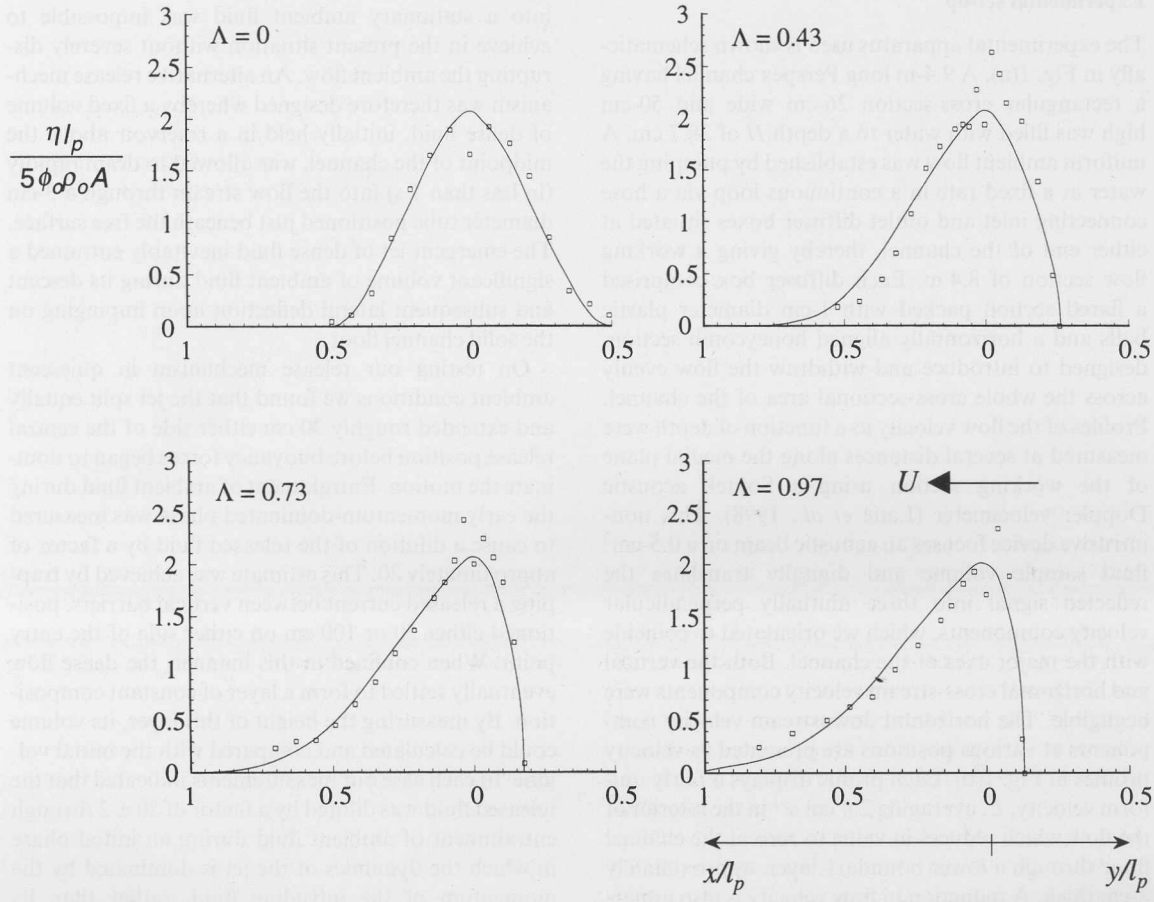

Fig. 5. Plots of the experimentally measured deposit profiles and the theoretical predictions for four different values of $\Lambda = 10UA/(V_s l_p^2)$.

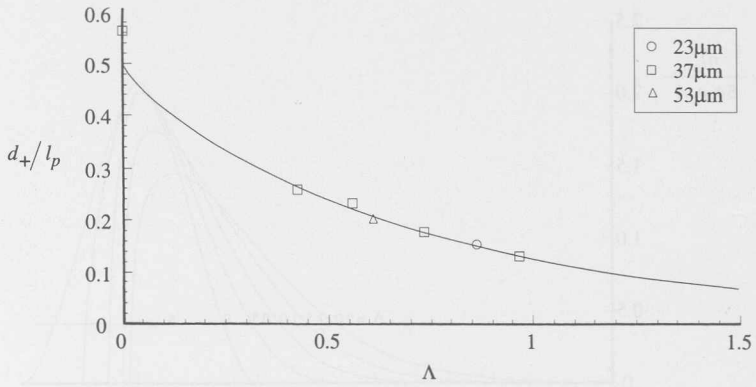

Fig. 6. The maximum non-dimensional upstream distance d_+/l_p as a function of $\Lambda = 10UA/(V_s l_p^2)$. The calculation of the theoretical curve is described in the text.

EXPERIMENTS

Experimental set-up

The experimental apparatus used is shown schematically in Fig. 1(a). A 9.4-m long Perspex channel having a rectangular cross-section 26-cm wide and 50-cm high was filled with water to a depth H of 28.7 cm. A uniform ambient flow was established by pumping the water at a fixed rate in a continuous loop via a hose connecting inlet and outlet diffuser boxes situated at either end of the channel, thereby giving a working flow section of 8.4 m. Each diffuser box comprised a flared section packed with 1-cm diameter plastic balls and a horizontally aligned honeycomb section, designed to introduce and withdraw the flow evenly across the whole cross-sectional area of the channel. Profiles of the flow velocity as a function of depth were measured at several distances along the medial plane of the working section using a Sontek acoustic Doppler velocimeter (Lane *et al.*, 1998). This non-intrusive device focuses an acoustic beam on a 0.5-cm^3 fluid sample volume and digitally translates the reflected signal into three mutually perpendicular velocity components, which we orientated to coincide with the major axes of the channel. Both the vertical and horizontal cross-stream velocity components were negligible. The horizontal downstream velocity components at various positions are presented as velocity profiles in Fig. 1(b). Each profile displays a fairly uniform velocity, $\bar{U}$, averaging 2.9 cm s^{-1} in the interior of the flow which reduces in value to zero at the channel floor through a lower boundary layer, approximately 2-cm thick. A reduction in flow velocity is also apparent as the free surface is approached. Integration of these flow profiles yielded an average volumetric flux of 1850 cm^3 s^{-1}, which corresponds to a Reynolds number of approximately 7000.

The conventional lock-release method of instantaneously initiating a gravity current of fixed volume into a stationary ambient fluid was impossible to achieve in the present situation without severely disrupting the ambient flow. An alternative release mechanism was therefore designed whereby a fixed volume of dense fluid, initially held in a reservoir above the midpoint of the channel, was allowed to drain rapidly (in less than 1 s) into the flow stream through a 3-cm diameter tube positioned just beneath the free surface. The emergent jet of dense fluid inevitably entrained a significant volume of ambient fluid during its descent and subsequent lateral deflection upon impinging on the solid channel floor.

On testing our release mechanism in quiescent ambient conditions we found that the jet split equally and extended roughly 30 cm either side of the central release position before buoyancy forces began to dominate the motion. Entrainment of ambient fluid during the early momentum-dominated phase was measured to cause a dilution of the released fluid by a factor of approximately 20. This estimate was achieved by trapping a released current between vertical barriers, positioned either 50 or 100 cm on either side of the entry point. When confined in this manner, the dense flow eventually settled to form a layer of constant composition. By measuring the height of this layer, its volume could be calculated and compared with the initial volume. In each case our measurements indicated that the released fluid was diluted by a factor of 20 ± 2 through entrainment of ambient fluid during an initial phase in which the dynamics of the jet is dominated by the momentum of the intruding fluid, rather than its buoyancy.

In the calculation of the length and time scales for

the compositional currents (Eqs (5) and (7)), the initial area, A, does not occur separately from the initial total buoyancy, $g'A$. The buoyancy is conserved under mixing and so the dilution described above does not affect the non-dimensionalization. However for the particle-driven currents, the initial area does occur separately from the total buoyancy (in Eq. (12) for example) and so a knowledge of the initial dilution is vital for the scaling of these experimental results.

Measurements were made of the horizontal distance to the front of the current from the release point as functions of time in both the downstream (x) and upstream (y) directions by marking the position of the nose of the current at 3-second intervals. In the case of particle-driven gravity currents, the final distribution of sedimented particles was measured by recovering the mass of particles within a 5-cm-wide strip across the width of the tank at various distances from the release point.

Compositional currents

Compositional currents of different initial densities were generated by releasing 2 litres of water containing 50 g, 200 g and 400 g of dissolved salt into the ambient flow, resulting in initial values of g' of 17.1, 64.4 and 121 cm s^{-2} respectively. Solutions of each concentration were also released into a quiescent ambient for comparison. The currents released into a uniform ambient flow advanced both upstream and downstream, but were markedly asymmetrical. In the downstream (x) direction, the current was noticeably thicker than its counterpart in a static environment, and propagated with an increased velocity. As distance from the release point increased, the velocity of the current gradually decreased to a value approaching 0.6 times the mean ambient velocity (see above). In the upstream (y) direction, the current was significantly retarded by the opposing ambient flow, and eventually came to rest. Prior to final arrest, the current profile was observed to undergo a transition from the typical head and tail of a gravity current intruding quiescent surroundings into a much thinner wedge-shape within the lower boundary layer. Once in this form, dense fluid was continually stripped away from the upper surface of the arrested wedge by the action of interfacial eddies.

In Fig. 2, we plot the relationships (9) and note that the agreement between the theoretical predictions and the experimental data is good. Hence the relationships (3) for the upstream and downstream position of the current can be used with confidence.

Particle-driven currents

Particle-driven gravity currents were generated by releasing well-mixed suspensions of silicon carbide particles in water. These particles are fairly monodisperse, non-cohesive and have a density $\rho_s = 3.217$ g cm^{-3}. As a precaution, a small amount of Calgon was added to the suspension to prevent particle agglomeration. Three different particle sizes were used, with mean diameters of 23, 37 and 53 μm. Details of the size distribution with each grade are reported in Huppert *et al.* (1991). For each particle size, experiments were run with four different initial particle masses of 50 g, 100 g, 200 g and 400 g suspended in 2 litres of water. Upon release, the particle-driven gravity currents propagated with decreasing velocity in both the x and y directions while simultaneously depositing a sediment layer over the channel floor until all the particles had settled out, whereupon the current ceased to exist.

Velocities of the current at any point achieved by each flow were observed to increase monotonically with increasing initial mass of suspended sediment, and the current attained progressively longer maximum distances from the release point with decreasing particle diameter. The currents released into an ambient flow were markedly elongated in the downstream direction. The development of an arrested wedge of dense fluid in the upstream direction was not as noticeable as that seen in the compositional currents, since particles quickly sedimented from thinned flows which are formed in the slow moving lower boundary layer of the opposing stream.

We plot in Fig. 3 the theoretical curves (Eqs 13b, c) and the experimental data, non-dimensionalized according to the scaling suggested by the box model. We note that the non-dimensionalization collapses the experimental data and that there is very good agreement with the theoretical predictions, again confirming the power of the box model approach. The relationship (13c) suggests that the position of the centroid should depend linearly on ΛT. However, as noted above, we are uncertain as to the exact value of U to use in the definition of Λ, although previous smaller studies (Simpson & Britter 1980) have indicated that $U = 0.6\bar{U}$, where $\bar{U}$ is the mean velocity in the channel. Figure 3(b) presents experimental data on the position of the centroid against $\Lambda T/U$. From the gradient of the fitted curve we find that $U = 1.8$ cm s^{-1} which corresponds to $U = 0.62\bar{U}$. In our experiments, the velocity in the boundary layer attains 62% of the mean ambient velocity at a distance of approximately

7 mm from the floor. Most of the currents were considerably thicker than this. It is our opinion that the ratio of around 0.6 (between U and $\bar{U}$) is independent of the thickness of the current as long as this is considerably larger than the thickness of the boundary layer.

Once all the particles had settled out, the final length of the deposited layer was recorded, and its mass distribution measured by 'vacuuming up' the sediment using a siphon tube within a 5 cm × 25 cm rectangular 'pastry cutter' placed over the layer at specific intervals. The mixture was collected in a beaker, the water decanted and the particles dried and weighed to determine the mass of deposit per unit area. As a check on the sampling method, the total mass of sediment was recovered by integrating the measured deposition profile and was generally found to be within 1% of the initial value. We compare some of the experimentally measured deposit profiles with the theoretical predictions for four values of Λ in Fig. 5. The agreement is seen to be very good and in particular the asymmetry predicted by the theory is accurately reflected by the data.

AXISYMMETRIC CURRENTS

We now develop a theoretical model of the radial spreading of an intrusion of relatively dense fluid within a uniform ambient flow. In the absence of an ambient flow, the dense fluid propagates radially away from its source. Its rate of propagation may be modelled using a box-model approach which has been demonstrated to yield good agreement with experimental measurements for both compositional currents (Huppert & Simpson, 1980) and particle-driven currents (Dade & Huppert, 1995; Bonnecaze *et al.*, 1995). In this section we extend the box-model analysis to incorporate the effect of a unidirectional flow. The spreading of dense fluid is no longer radial and we calculate the locus of points which correspond to the position of the front of gravity current. The gravity current never reaches positions outside this locus.

Axisymmetric models of gravity currents may be equally well applied to flows within an angular sector, provided that the boundaries of the sector have only a negligible influence. (This is equivalent to requiring that the lengthscale associated with the gravity current be much larger than that of the boundary layer.) Hence this study may be applied to discharges of dense fluid at the boundary of a relatively wide channel flow, such as a river or an estuary.

Guided by the success of the approach outlined above, in the following we develop box models of gravity currents driven by a compositional difference or the suspension of particles in the presence of a mean flow. Our emphasis is to establish the extent of the region within which the intrusion will propagate and, for particle-driven gravity currents, to calculate the distribution of the deposited sediment.

Compositional currents

We consider the instantaneous intrusion of a finite volume of fluid with a density, ρ_c into an ambient fluid of a lower density, ρ_a. The intruding fluid spreads along the horizontal boundary underlying the ambient fluid, its motion being driven by gravity. The ambient fluid flows uniformly in a horizontal direction. We define horizontal coordinate axes such that the x-axis is aligned with this uniform flow and the y-axis is perpendicular to the flow. As in the two-dimensional case, it is convenient to formulate the equations governing the evolution of the flow in a frame of reference which moves with the velocity of the centroid of the intrusion. In this frame the gravity current spreads radially in the form of a uniform disk whose radius and height change with time. Denoting the radial distance from the centroid by r, the conservation of fluid volume of the current may be expressed by

$$r^2 h = V, \tag{18}$$

where h is the height of the current and V is twice the volume per unit (radian) angle, which remains constant during the evolution of the current. (The total volume is πV.) The rate of radial expansion of the gravity current in this moving frame is given by

$$\frac{\mathrm{d}r}{\mathrm{d}t} = \mathrm{Fr}(g'h)^{\frac{1}{2}}, \tag{19}$$

where $g' \equiv (\rho_c - \rho_a)g/\rho_a$ is the reduced gravity of the current and Fr is the frontal Froude number, which is assumed constant. Substitution of Eq. (18) into Eq. (19) and integration, subject to the initial condition that $r = 0$ at $t = 0$, yields

$$r = (2\mathrm{Fr}(g'V)^{\frac{1}{2}}t)^{\frac{1}{2}}. \tag{20}$$

Denoting the position of the centroid by $\bar{x}$ we write

$$\bar{x} = Ut, \tag{21}$$

where U is the velocity experienced by the gravity current in response to the ambient flow. (For the

two-dimensional gravity currents it was established that U was 0.6 of the mean flow.) At this stage it is convenient to identify the following time and length scales which may be used to non-dimensionalize the relationships (20) and (21),

$$t_a = 2\mathrm{Fr}(g'V)^{\frac{1}{2}}/U^2 \quad \text{and} \quad r_a = 2\mathrm{Fr}(g'V)^{\frac{1}{2}}/U. \tag{22}$$

The timescale t_a corresponds to the time at which the velocity of the gravity-driven motion and the uniform flow are comparable, while the lengthscale r_a is the downstream distance moved after this time. Writing the dimensionless variables as $R_a = r/r_a$, $\bar{X}_a = \bar{x}/r_a$ and $T_a = t/t_a$, we find that

$$R_a = T_a^{\frac{1}{2}} \quad \text{and} \quad \bar{X}_a = T_a. \tag{23}$$

Hence the boundary of the spreading gravity current, expressed in terms of a fixed frame of reference in which X_a and Y_a are dimensionless horizontal co-ordinates, is given at any particular time by

$$(X_a - \bar{X}_a)^2 + Y_a^2 = R_a^2. \tag{24}$$

We may therefore determine the boundary of the region within which the current propagates. In parametric form it is given by evaluating the full derivative of Eq. (24) with respect to T_a and setting $\mathrm{d}X_a/\mathrm{d}T_a$ and $\mathrm{d}Y_a/\mathrm{d}T_a$ to zero, which yields

$$X = \tau - \tfrac{1}{2} \quad \text{and} \quad Y^2 = \tau - \tfrac{1}{4}. \tag{25}$$

where (X, Y) are non-dimensional co-ordinates. In these non-dimensional variables the region is given by the parabola

$$Y^2 = X + \tfrac{1}{4}. \tag{26}$$

Particle-driven currents

A conceptually similar model may be developed to describe the gravity-driven flow of a particle-laden intrusion within a uniformly flowing ambient. This motion, however, is complicated by the sedimentation of particles from the current to the lower boundary which progressively reduces the density, and hence the buoyancy-induced propagation velocity is also reduced. Box-model equations for the conservation of fluid volume and the rate of radial propagation may be formulated in a frame of reference moving with the centroid. They yield

$$r^2 h = V \tag{27}$$

and

$$\frac{\mathrm{d}r}{\mathrm{d}t} = \mathrm{Fr}(g'_p \phi h)^{\frac{1}{2}}. \tag{28}$$

Particle settling is modelled in an analogous manner to the two-dimensional case

$$\frac{\mathrm{d}}{\mathrm{d}t}(V\phi) = -V_s \phi r^2. \tag{29}$$

Thus from Eqs (28) and (29) we find that

$$\left(\frac{\phi}{\phi_0}\right)^{\frac{1}{2}} = 1 - \frac{V_s r^4}{8\mathrm{Fr}(g'_p \phi_0 V^3)^{\frac{1}{2}}}, \tag{30}$$

where ϕ_0 is the initial volume fraction of particles. Hence we use the length and timescales

$$r_p = \left[\frac{8\mathrm{Fr}(g'_p \phi_0 V^3)^{\frac{1}{2}}}{V_s}\right]^{\frac{1}{4}} \quad \text{and} \quad t_p = \frac{4V}{V_s r_p^2} \tag{31}$$

to non-dimensionalize the governing equations. The lengthscale r_p corresponds to the radius of the particle-driven intrusion at which the volume fraction vanishes. Defining the dimensionless variables as $R_p = r/r_p$, $\bar{X}_p = \bar{X}/r_p$, $T_p = t/t_p$ and $\Phi = \phi/\phi_0$ and integrating the equations of motion, we obtain

$$R_p = \tanh^{\frac{1}{2}} T_p, \tag{32a}$$

$$\Phi = \mathrm{sech}^4 T_p \tag{32b}$$

and

$$\bar{X}_p = \lambda T_p. \tag{32c}$$

In these expressions there remains a single dimensionless parameter,

$$\lambda = \frac{4UV}{r_p^3 V_s}, \tag{33}$$

which measures the magnitude of the horizontal flux of fluid against the vertical settling flux. (It is analogous to the parameter Λ introduced above.) These equations govern the temporal evolution of the radius and volume fraction of particles of the particle-laden cloud in a frame moving with the centroid. In a fixed frame of reference, the perimeter of the cloud is given by

$$(X - \lambda T_p)^2 + Y^2 = R_p^2. \tag{34}$$

The region within which the gravity current propagates can now may be calculated. It corresponds to the region within which particles are deposited from the

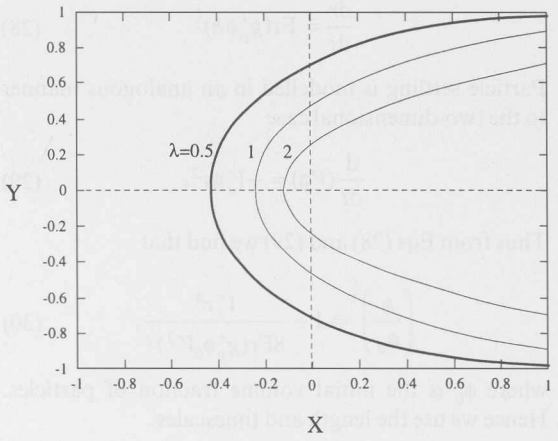

Fig. 7. The boundary of the region within which the particle-driven gravity current propagates for $\lambda = 0.5, 1, 2$.

current. The boundary of this region, in parametric form, is given by

$$X = -\frac{\operatorname{sech}^2\tau}{2\lambda} + \lambda\tau \tag{35a}$$

and

$$Y = \left(\tanh\tau - \frac{\operatorname{sech}^4\tau}{4\lambda^2}\right)^{\frac{1}{2}}. \tag{35b}$$

We plot these loci in Fig. 7. The maximum upstream distance, X_m, propagated by the current may be calculated by finding the value of the parameter τ for which $Y = 0$ (Eq. 35b) which is then substituted into (Eq. 35a). The distance, X_m, may be evaluated in the regimes of weak ($\lambda << 1$) and strong ($\lambda >> 1$) ambient flows relative to the initial buoyancy-induced speed of propagation. We find that

$$X_m = -1 + \tfrac{1}{2}\lambda(1 + \ln 2 - \ln\lambda) - \tfrac{1}{4}\lambda^2 + O(\lambda^4) \quad (\lambda << 1) \tag{36a}$$

$$= -\frac{1}{4\lambda} + \frac{1}{192\lambda^5} + O\left(\frac{1}{\lambda^9}\right) \quad (\lambda >> 1). \tag{36b}$$

The distribution of the deposit arising from the flow of the particle-driven intrusion may be calculated in a manner analogous to the two-dimensional case. It is assumed that the particles sediment out of the flow uniformly throughout the area covered by the particle-laden cloud. Therefore at a dimensional location (x, y) the deposit measured in mass per unit area is given by

$$\eta(x, y) = t_p \rho_p V_s \phi_0 \int_{T_s}^{T_f} \Phi \, d\tau, \tag{37}$$

where T_s and T_f are the dimensionless times at which sedimentation starts and finishes at this particular location. If the dimensionless position, (X, Y), falls outside of the locus given by Eq. (35a, b) there is no deposit. Conversely if the position lies within the locus the deposit is given implicitly by

$$\eta(X, Y) = \frac{4V\rho_p}{r_p^2}\left[R_p^2 - \frac{R_p^6}{3}\right]_{R_s}^{R_p}, \tag{38}$$

where the terms within the square bracket are evaluated at the upper and lower limits of R_f and R_s which are the dimensionless radii of the intrusion corresponding to the times T_f and T_s, respectively. In Fig. 8 we plot contours of the deposit, noting that the degree of asymmetry is a function of the parameter λ.

DISCUSSION AND CONCLUSIONS

We have investigated the flow and dispersion of small, heavy particulate matter in a uniform horizontal flow. We analysed the current using the box model approximation which yields a simple analytic formulation. We considered both two dimensional (line source) and axisymmetric (point source) releases of the particles and experimentally verified our quantitative results for the former geometry.

In the two-dimensional situation the flow varies with the parameter $\Lambda = 10UA/(l_\infty^2 V_s)$, as given by Eq. (14), which represents a ratio of the advective flux of the flow to the downward particle flux within the flow. The maximum upstream penetration is given (to a high degree of approximation) by Eq. (17). The particle concentration within the current as a function of time and position is given by Eq. (13) and the final deposition density by Eq. (16). In the situation where the particle dispersion is unconfined (axisymmetric), the governing parameter is $\lambda = 4UV/(r_p^3 V_s)$ and the horizontal extent of the current is given by Eq. (35) with the deposit density represented by Eq. (38).

The upstream penetration against the main flow can have important (and to some people surprising) consequences. Ms Mary-Louise Timmermans (HEH's graduate student) tells us that when she and her medical father visited Dawson City, Yukon in Northern Canada, he was approached by the town authorities about an outbreak of disease which seemed to occur after the town's sewerage outlet was discharged into

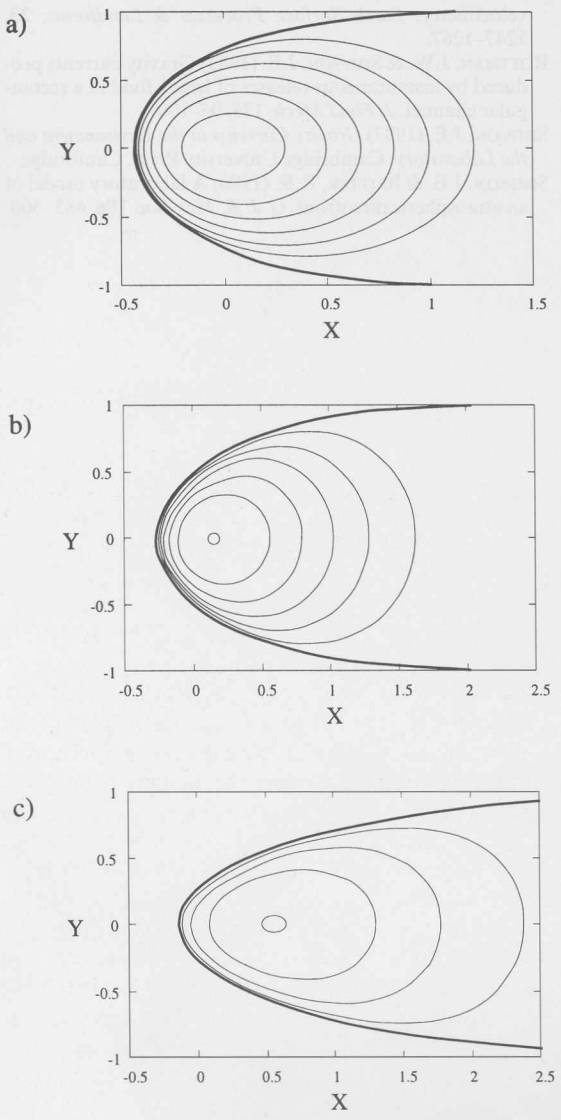

Fig. 8. (a) Contours of the distribution of the deposit per unit area and the (thicker) bounding curves for (a) $\lambda = 0.5$, (b) $\lambda = 1$ and (c) $\lambda = 2$. The deposit has been non-dimensionalized with respect to $4V\rho_p/r_p^2$. The contours are shown at intervals of 0.1 in the range 0–0.6 for (a) and (b), and 0–0.4 for (c).

the town river but *downstream* of the water-supply intake. Ms Timmermans had no difficulty in explaining the problem!

In order to give some quantitative feeling for our results, consider now the following examples. For each of them consider the particulate matter to be 20 μm in diameter and have an excess density of 1 g cm^{-3}, which implies a settling velocity in water of 0.022 cm s^{-1}. A suspension of such particles with concentration 5% by volume and cross-section (in the two-dimensional situation) of 100 m^2 leads to a length-scale l_∞ of 1.1 km. In a uniform flow (such as the tides, for example) of 10 cm s^{-1}, $\Lambda = 0.25$ and the particle-laden current propagates upstream over a distance d_+ of 200 m. If, instead, a total of 10^3 m^3 of suspension of volume concentration 5% is instantaneously released from a point source in the same uniform flow the radial scale r_p is 180 m, $\lambda = 0.2$ and the upstream penetration length is 120 m.

ACKNOWLEDGEMENTS

We are very grateful to Dr. Mark Hallworth for helping us with the experiments and their analysis and for preparing the figures for this publication. A.J.H. acknowledges the support of a grant from the Nuffield Foundation (NUF-NAL).

REFERENCES

BAKER, E.T., GERMAN, C.R. & ELDERFIELD, H. (1995) Hydrothermal plumes over spreading-center axes: global distributions and geological inferences. Physical, chemical, biological and geological interactions within seafloor hydrothermal systems. *Geophys. Monograph* **91**, 47–71.

BENJAMIN, T.B. (1968) Gravity currents and related phenomena, *J. Fluid Mech.* **88**, 223–240.

BONNECAZE, R.T., HALLWORTH, M.A., HUPPERT, H.E. & LISTER, J.R. (1995) Axisymmetric particle-driven gravity currents. *J. Fluid Mech.* **294**, 93–121.

BONNECAZE, R.T., HUPPERT, H.E. & LISTER, J.R. (1993) Particle-driven gravity currents. *J. Fluid Mech.* **250**, 339–369.

DADE, W.B. & HUPPERT, H.E. (1994) Predicting the geometry of channelised deep-sea turbidites. *Geology* **22**, 645–648.

DADE, W.B. & HUPPERT, H.E. (1995) Runout and fine-sediment deposits of axisymmetric turbidity currents. *J. geophys. Res.* **100**, 18597–18609.

ERNST, G., HOGG, A.J. & HUPPERT, H.E. (2001) Deposit densities resulting from explosive umbrella clouds influenced by the wind. (In preparation.)

HALLWORTH, M.A., HOGG, A.J. & HUPPERT, H.E. (1998) Effects of external flow on compositional and particle gravity currents. *J. Fluid Mech.* **359**, 109–142.

HOGG, A.J., UNGARISH, M. & HUPPERT, H.E. (2000) Particle-driven gravity currents: asymptotic solutions and box models. *Eur. J. Mech.* **19**, 139–165.

HUPPERT, H.E. (1997) Buoyancy effects in fluids. Part III Mathematical Tripos Examination.

HUPPERT, H.E. (1998) Quantitative modelling of granular suspension flows. *Phil. Trans. R. Soc. A* **356**, 2471–2496.

HUPPERT, H.E. & SIMPSON, J.E. (1980) The slumping of gravity currents. *J. Fluid Mech.* **99**, 785–799.

HUPPERT, H.E., KERR, R.C., LISTER, J.R. & TURNER, J.S. (1991) Convection and particle entrainment driven by differential sedimentation. *J. Fluid Mech.* **226**, 349–369.

LANE, S.N., BIRON, P.M., BRADBROOK, K.F., BUTLER, J.B., CHANDLER, J.H., CROWELL, M.D., MCLELLAND, S.J., RICHARDS, K.S. & ROY, A.G. (1998) Measurements of river channel flow processes using acoustic Doppler velocimetry. *Earth Surface Processes & Landforms*, **23**, 1247–1267.

ROTTMAN, J.W. & SIMPSON, J.E. (1983) Gravity currents produced by instantaneous releases of heavy fluid in a rectangular channel. *J. Fluid Mech.* **135**, 95–100.

SIMPSON, J.E. (1997) *Gravity Currents in the Environment and the Laboratory*. Cambridge University Press, Cambridge.

SIMPSON, J.E. & BRITTER, R.E. (1980) A laboratory model of an atmospheric mesofront. *Q. J. R. Met. Soc.* **106**, 485–500.